Self-propelled motion of induced-charge electrophoretic Janus particles in viscoelastic fluids

Keita Saito,[1,2] Ryunosuke Kawano,[1] Chisato Sadamatsu,[1] Yasutaka Iwashita,[3] and Yasuyuki Kimura[1,*]

[1]*Department of Physics, School of Science, Kyushu University, 744 Motooka, Nishi-ku, Fukuoka 819-0395, Japan*

[2]*RIKEN Center for Emergent Matter Science, 2-1 Hirosawa, Wako, Saitama 351-0198, Japan*

[3]*Department of Physics, School of Science, Kyoto Sangyo University, Motoyama Kamigamo, Kita-ku, Kyoto 603-8555, Japan*

(Received 20 November 2024; accepted 10 March 2025; published 10 April 2025)

Swimming micro-objects exist in viscoelastic fluids. Elucidating the effect of viscoelasticity on the motion of these objects is important for understanding their behavior. Since the mechanical response of viscoelastic fluids depends on the temporal deformation rate exerted by a moving object, it is necessary to control their speed over a wide range to examine the effect of viscoelasticity. In this study, we examined the motion of Janus particles self-propelled by induced charge electrophoresis over a wide range of speeds in semidilute polymer solutions. In our system, the motion of Janus particles changed from active Brownian motion to stationary rotation as the speed increased. The torque for stationary rotation originates from the difference between the direction of self-propulsion and that of the time-delayed restoring force from the polymer solution, which has been reported in another self-propelled particle system. The switch from active Brownian motion to stationary rotation at different polymer concentrations can be explained by the Weisenberg number, which is defined as the ratio of the relaxation time of the polymer network to the travel time of the Janus particle to its size. The results of this study will lead to a better understanding of the motion of self-propelled micro-objects in viscoelastic fluids.

DOI: 10.1103/PhysRevE.111.045409

I. INTRODUCTION

Microorganisms, such as bacteria and plankton, are often exposed to viscoelastic fluids in nature [1,2]. Biological processes, such as biofilm formation, occur in viscoelastic fluids [3]. Understanding their motion in viscoelastic fluids is important for elucidating their biological phenomena.

Viscoelastic fluids differ from Newtonian fluids because their mechanical responses depend on the temporal rate of deformation [4]. The response is characterized by the Weissenberg number W_{i}, which represents the relative ratio between the elastic and viscous components [5]. The motility of *Escherichia Coli* (*E. coli*) differs between Newtonian and viscoelastic fluids [6,7]. Although *E. coli* exhibits run-and-tumble motion in Newtonian fluids, its tumbling motion is suppressed in viscoelastic fluids because of its elastic response. The elasticity of the surrounding fluid plays an important role in the movement of microswimmers from self-propelled colloidal particles to microorganisms in viscoelastic fluids [2]. Since the temporal rate of deformation is determined by the swimming speed of the microswimmers, it is necessary to control the swimming speed to clarify the effects of viscoelasticity on their motion. Artificial microswimmers, whose swimming speed can be controlled, are useful for studying viscoelastic effect [8,9].

Janus particles are typical artificial microswimmers that are colloidal particles with two distinct surfaces or regions that exhibit different properties [10,11]. Janus particles can self-propel through an asymmetric response to external fields, and the methods of their self-propulsion depend on the combination of surface properties [12]. In Newtonian fluids, many types of self-propelled Janus particles exhibit active Brownian motion [13]. The active Brownian motion is ballistic within the time characterized by the rotational diffusion coefficient, whereas the motion becomes diffusive in the region above the characteristic time.

To date, few self-propelled particle systems have been used to study the effects of viscoelasticity on particle motion [14–16]. An example is a system with self-diffusiophoretic Janus particles activated by light irradiation [14,15]. The hemispheres of the particles were covered with gold or carbon caps. In this system, self-diffusiophoresis is induced by phase separation around the cap caused by the temperature increase in the cap due to light absorption [17,18]. This self-propelled particle, with a speed above a certain threshold, exhibits stationary rotation in semidilute polymer solutions [15]. Another example is a self-diffusiophoretic particle system, in which an asymmetric chemical reaction around a Janus particle with a platinum cap in H_2O_2 solution induces self-diffusiophoresis [13,19]. This self-propelled particle does not exhibit stationary rotation in viscoelastic fluids but exhibits active Brownian motion, as in Newtonian fluids [16]. In these two studies, the important parameter for characterizing self-propelled motion is still unclear, and a more systematic study on the effect of viscoelasticity is required.

Janus particles with metal caps in electrolyte solutions can be self-propelled by induced charge electrophoresis (ICEP) under an alternating electric field [20,21]. Since the speed of self-propulsion by the ICEP is dependent on the frequency and strength of the externally applied electric field $\boldsymbol{E}$, controlling the speed is easier when compared to the aforementioned

*Contact author: kimura@phys.kyushu-u.ac.jp

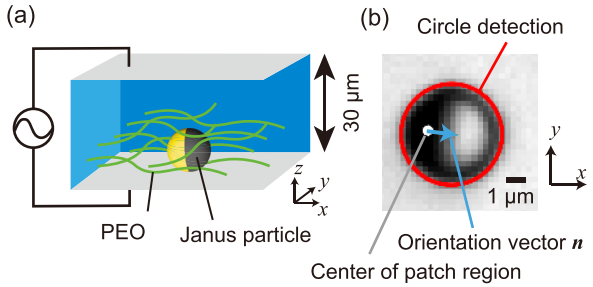

FIG. 1. Metal-dielectric Janus particles dispersed in a PEO solution. (a) Schematic of the sample cell. The green line represents a polymer. (b) Detection of the center of a Janus particle and metal patch region. The red circle represents the outline of the Janus particle. The white dot represents the center of the patch region. The blue arrow represents the orientation vector $\boldsymbol{n}$ of the particle. The scale bar is 1 μm.

two methods. Additionally, because the speed is proportional to the square of the amplitude of the electric field, it can be controlled over a wide range [21]. Therefore, ICEP is a suitable method for examining the effects of viscoelastic fluids on microswimmers.

In this study, we controlled W_i over a wide range, between 10^{-2} and 10^{1}, by varying the polymer concentration and speed to examine the relationship between the mechanical response of the polymer solution and motion of the Janus particle. The translation and rotation of the Janus particle were separately identified, and their dependence on W_i was discussed.

II. EXPERIMENTAL SETUP

The Janus particles we used were silica particles (Hyprecica, UEXC) with radius $a = 2.5\,\mu$m half-coated with chromium (Cr). Janus particles dispersed in an aqueous solution of polyethylene oxide (PEO) (Sigma-Aldrich, Molecular weight $= 10^6$) at a mass concentration C_m were injected into the sample cell facing two transparent indium tin oxide (ITO) electrodes (GEOMATEC) coated with a 25-nm-thick SiO_2 layer to prevent the Janus particles from sticking to the cell bottom. We applied the sinusoidal electric field with a frequency of 3 kHz, where self-propulsion speed shows maximum value. The two electrodes are separated by a 30-μm thick spacer (double-sided tape), as shown in Fig. 1(a). Typically, there were two or three particles in an area with dimensions of approximately 600 μm × 600 μm (corresponding to the image size). Therefore, collisions between particles are rarely observed. Since the particle concentration is diluted, the effect of other particles on the motion of the Janus particles should be negligible in our system. Electrolysis of aqueous solutions did not occur during this experiment. Owing to individual differences in Janus particles, the average speed differs between the particles even for the same E. The distribution of the speed for each concentrations is presented in Appendix A. The distribution is relatively wide. A similar difference in Janus particles self-propelled by ICEP was reported in previous studies [22,23]. The Janus-particle equator is aligned to be parallel to E [21]. Since the Janus particles were heavier than the solution, they settled at the bottom, and their motion was confined to a two-dimensional plane perpendicular to E.The motion of the Janus particles was observed from below using an inverted optical microscope (Eclipse Ti, Nikon) with a ×10 or ×20 objective lens (Plan Fluor, Nikon) depending on the self-propulsion speed v of the Janus particles (the estimation of v will be described later): ×10 objective lens for $v \gtrsim 2$ μm/s and ×20 objective lens for $v \lesssim 2$ μm/s. Images of the Janus particles were captured using a CMOS camera (Orca-Flash 4.0, Hamamatsu, 2048 × 2048 pix^2). The sampling time of the CMOS camera was varied depending on v: 50 ms for $v \gtrsim 2$ μm/s and 0.2 s for $v \lesssim 2$ μm/s.

The two-dimensional position $\boldsymbol{r}$ of the Janus particles is determined by circle detection, as shown in Fig. 1(b). The center of the patch region (Cr cap) was also detected in the binarized image of the Janus particles. The orientation vector $\boldsymbol{n}$ of the Janus particle is defined as the vector connecting the center of the outline circle and the center of the patch, as indicated by the blue arrow in Fig. 1(b). θ is the angle between the orientation vector and the x-axis. Because the direction of the self-propulsion force is in the same direction as $\boldsymbol{n}$, the direction of translational motion of the Janus particle self-propelled by the ICEP is the same as $\boldsymbol{n}$ (self-propulsion velocity $\boldsymbol{v} = v\boldsymbol{n}$) [21].

III. RESULTS AND DISCUSSIONS

A. Self-propelling mode

We first explain the motion of a Janus particle in a Newtonian fluid (water) before explaining its motion in viscoelastic fluids. The Janus particles exhibited active Brownian motion. Typical trajectories of the Janus particles in water at $E = 0.15 - 0.32\,$V/μm in approximatel 10 s are shown in Fig. 2(a). Figure 2(b) shows the dependence of mean-squared displacement (MSD) $\langle \Delta \boldsymbol{r}^2 \rangle$ of the two-dimensional trajectories of Fig. 2(a) on the elapsed time Δt. The observed motion in water corresponded to the ballistic region of active Brownian motion. Furthermore, v was estimated from the MSD in this region, $\langle \Delta \boldsymbol{r}^2 \rangle = (v\Delta t)^2$.

In the PEO solution with $C_m = 1.0\,$wt%, the motion of the Janus particles differed from that in water, especially for large E. At $E = 0.30$ and 0.32 V/μm, circular orbits were observed. The typical trajectories of Janus particles are shown in Fig. 2(c), where the measurement time is approximately 800 s. The direction of rotation differed for each particle. Although Janus particles can reverse their direction of rotation, this reversal was rarely observed during the measurement period. We calculate the MSD of the two-dimensional trajectories in Fig. 2(c) as shown in Fig. 2(d). For small Δt, the slope of the MSD increases slightly at $E = 0.30$ and 0.32 V/μm as shown in Fig. 2(d). At $E = 0.15$ and 0.25 V/μm, the slope of the MSD increases from less than unity to two. This increase indicates the change from subdiffusive to ballistic motion as Δt increases. This subdiffusion at small Δt is a characteristic of a viscoelastic solution [24]. At large Δt, the MSDs at $E = 0.30$ and 0.32 V/μm showed an oscillatory dependence on Δt, which corresponds to the circular orbits shown in Fig. 1(c). At $E = 0.25$ V/μm, the MSD curve implies the onset of oscillation. At $E = 0.15$ V/μm, the slope does not change significantly. From the MSD in Fig. 2(d), it is difficult

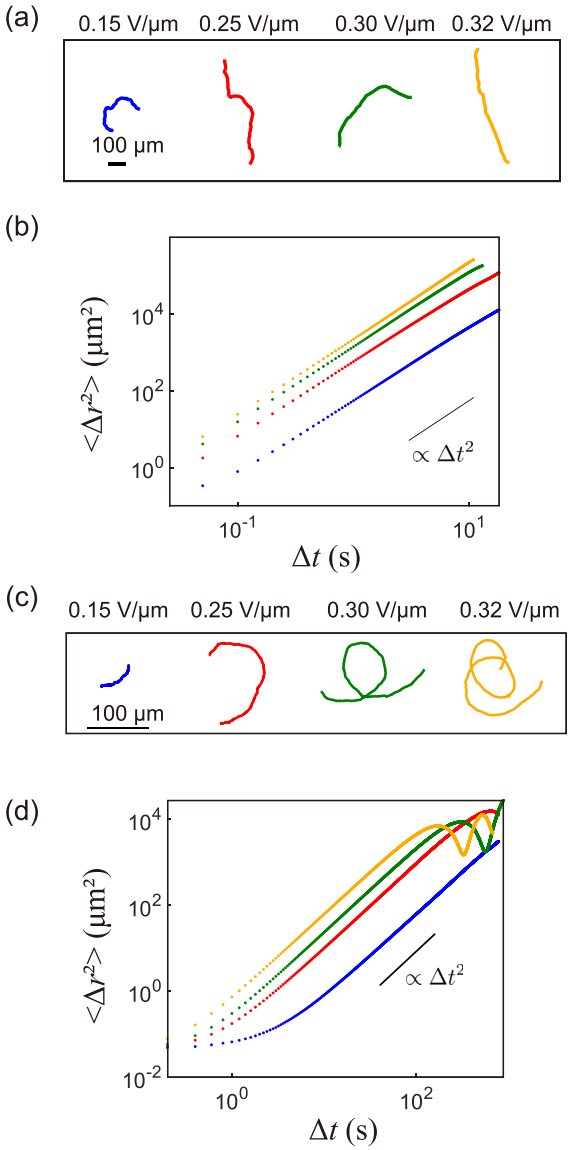

FIG. 2. Motion of Janus particles in water (a), (b) and 1.0 wt% PEO solution (c), (d). (a) Two-dimensional trajectories in water at different E values ($0.15 - 0.32$ V/μm). The observation time was ∼10 s. The scale bar is 100 μm. (b) Dependence of mean-squared displacement (MSD) $\langle \Delta r^2 \rangle$ evaluated from the two-dimensional trajectories of (a) on the elapsed time Δt. The colors respectively correspond to those of the trajectories in (a). MSD is proportional to $(\Delta t)^2$. (c) Two-dimensional trajectories in 1.0 wt% PEO solution at different E values (0.15–0.32 V/μm). The observation time was ∼800 s. The scale bar is 100 μm. (d) Dependence of MSD on Δt in PEO solution. The colors respectively correspond to those of the trajectories in (c). MSD is proportional to $(\Delta t)^2$ at the middle time range.

to determine whether the mode at $E = 0.15$ V/μm differs from the active Brownian motion.

Since the direction of propulsion is determined by particle orientation θ, the rotational motion of the Janus particle should be characterized by θ. The time evolution of the angular displacement $\Delta\theta$ for the trajectories shown in Fig. 2(c) was analyzed to evaluate the rotation quantitatively as shown

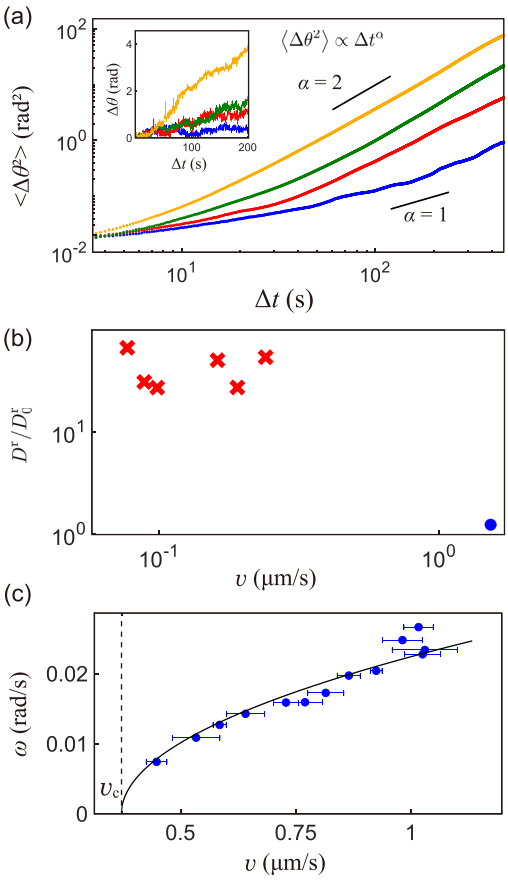

FIG. 3. Rotational motion of Janus particles in 1.0 wt% PEO solution. (a) Dependence of mean-squared angular displacement $\langle \Delta\theta^2 \rangle$ of a Janus particle on the time elapsed (Δt) at different values of v (blue: 0.1 μm/s ($E = 0.15$ V/μm), red: 0.3 μm/s ($E = 0.25$ V/μm), green: 0.5 μm/s ($E = 0.30$ V/μm) and yellow: 0.8 μm/s ($E = 0.32$ V/μm)). The lower and upper solid lines are proportional to Δt and $(\Delta t)^2$, respectively. The inset shows the time evolution of $\Delta\theta$. (b) D^r/D_0^r ratio in water and 1.0 wt% PEO solution. (blue dots: water, red crosses: PEO solution). D_0^r is calculated by $D_0^r = k_B T/8\pi\eta_0 a^3$ with $\eta_0 = 8.9 \times 10^{-4}$ Pa s (water) and $\eta_0 = 0.46$ Pa s (1.0 wt% PEO solution). (c) Variation in angular frequency ω with v for a Janus particle. The solid line represents the best-fitted curve representing Eq. (3) with $v_c = 0.37$ μm/s and $\tau = 58$ s. The dashed line represents v_c.

in the inset of Fig. 3(a). Since v is an important parameter for the mechanical response of viscoelastic fluids, we focused on v as opposed to E.

The rotation of the self-propelled Janus particle in the PEO solution differs from thermal diffusion such as the rotation in water. Figure 3(a) shows the dependence of mean-squared angular displacement (MSAD) $\langle \Delta\theta^2 \rangle$ on time elapsed Δt in the 1.0 wt% PEO solution. At $v = 0.3$, 0.5 and 0.8 μm/s, the slope increased from less than unity to approximately two, indicating that the rotational motion changed from subdiffusive to stationary rotation at a constant angular frequency ω, $\langle \Delta\theta^2 \rangle = (\omega \Delta t)^2$, as Δt increased. At $v = 0.1$ μm/s, the slope of $\langle \Delta\theta^2 \rangle$ gradually increased with Δt to unity. These types of changes in slope differ from the thermally diffusive rotation in Newtonian fluids [13]. The subdiffusive rotation at

small Δt is a characteristic of a viscoelastic solution similar to the subdiffusive translational motion of a passive colloidal particle in viscoelastic fluids [24], which is observed in our results shown in Fig. 2(d). There is a possibility that the slope at $v = 0.1$ μm/s is greater than unity outside the observation time window ($\Delta t \gtrsim 800$ s), which will be discussed later.

We examined the rotation of the Janus particle in large Δt. Since the slope is constant in $\Delta t \gtrsim 200$ s, we focus on MSAD in $\Delta t \gtrsim 200$ s. To investigate the rotation quantitatively, the power index α for $\langle \Delta\theta^2 \rangle \propto (\Delta t)^\alpha$ is estimated by MSAD. For small v, $v \lesssim 0.3$ μm/s, the typical rotation is diffusive. For $v = 0.1$ μm/s in Fig. 3(a), $\alpha = 1.2$. Here, we regard $\alpha = 0.8 - 1.2$ as diffusive rotation. In this diffusive region, we discuss D_r/D_0^r in water and PEO solution, where D_r is the effective rotational diffusion coefficient and D_0^r is the rotational diffusion coefficient based on the Stokes-Einstein relation. Regarding $\alpha = 0.8 - 1.2$ as $\alpha = 1$, D_r is evaluated from $\langle \Delta\theta^2 \rangle$ with $\langle \Delta\theta^2 \rangle = 2D_r \Delta t$. Furthermore, D_0^r is expressed as $D_0^r = k_B T/8\pi\eta_0 a^3$ where k_B is the Boltzmann constant, T is the absolute temperature and η_0 is the zero-shear viscosity of a surrounding solution. Estimation of η_0 for the PEO solution is presented in Appendix B. Furthermore, D_r/D_0^r of multiple Janus particles in the PEO solution becomes an order of magnitude larger than that in water as shown in the red crosses of Fig. 3(b). This enhancement is attributed to the fluctuating flow around the self-propelled particles in viscoelastic fluids [25]. Acceleration of the rotational diffusion of active particles in crowded environments has been reported not only in semidilute polymer solutions but also in colloidal dispersions near the glass transition [14,26]. In water, the D^r/D_0^r ratios are close to unity, as indicated by the blue points in Fig. 3(b).

At large v, $v \gtrsim 0.5$ μm/s, Janus particles typically exhibit stationary rotation: For $v = 0.8$ μm/s in Fig. 3(a), $\alpha = 2.0$. Specifically, we regard $\alpha = 1.8 - 2.2$ as stationary rotation. Regarding $\alpha = 1.8 - 2.2$ as $\alpha = 2$, ω is estimated by MSAD of the particles with $\langle \Delta\theta^2 \rangle = (\omega \Delta t)^2$. Under the condition that the Janus particle exhibits stationary rotation, we measured the variation of ω with v for a single Janus particle by changing E, as shown in Fig. 3(c). Furthermore, ω increases with v, and the similar dependence of ω on v is reported for self-diffusiophoretic Janus particles by light irradiation in semidilute polymer solutions [15].

B. Analysis of rotational motion

A moving particle in a semidilute polymer solution is subjected to not only viscous resistance but also the elastic force of the polymer solution. Narinder *et al.* [15] discussed the stationary rotation by considering the delayed elastic force of a polymer solution. In the following section, the outline of the theoretical model is explained, and our results are compared with those of the model.

The viscoelastic drag force $\boldsymbol{F}(t)$ acting on a particle moving at velocity $\boldsymbol{v}$ is expressed as $\boldsymbol{F}(t) = v \int_{-\infty}^{t} \Gamma_T(t - t')\boldsymbol{n}(t')dt'$, where $\boldsymbol{v}(t) = v\boldsymbol{n}(t)$, $\Gamma_T(t) = 6\pi a G(t)$ is the memory friction kernel, and $G(t)$ is the stress-relaxation modulus of the solution. For a semidilute polymer solution, $G(t)$ is expressed as [15,27]:

$$G(t) = 2\eta_\infty \delta(t) + \left(\frac{\eta_0 - \eta_\infty}{\tau} \right) e^{-t/\tau}, \tag{1}$$

where η_∞ is the instantaneous viscosity, τ is the relaxation time of the polymer network, and $\delta(t)$ is the Dirac's delta function. Since the direction of $\boldsymbol{F}(t)$ is determined by the previous $\boldsymbol{n}(t')$ ($t' < t$), misalignment between the directions of $\boldsymbol{F}(t)$ and $\boldsymbol{n}(t)$ could occur because $\boldsymbol{n}$ changes owing to the fluctuating flow around the self-propelled particle as mentioned above [14]. The misalignment induces torque $\boldsymbol{T} = (T_x, T_y, T_z)$, which is expressed as [15]:

$$\boldsymbol{T} = -\mu a v \int_{-\infty}^{t} \Gamma_T(t - t')\boldsymbol{n}(t) \times \boldsymbol{n}(t')dt', \tag{2}$$

where μa is the effective length of the lever arm, and μ is the adjustable parameter.

Since the boundary between the Cr and silica surfaces of our particles was in a plane parallel to the direction of the electric field, we only consider the rotation of the particles around the z-axis. Assuming that ω is constant, the balance between the viscous torque $\int_{-\infty}^{t} \Gamma_R(t - t')\omega(t')dt'$ with the memory friction kernel for the angular friction $\Gamma_R = 8\pi a^3 G(t)$ and torque $T_z(t)$ caused by the time-delayed force leads to [15]:

$$\omega = \begin{cases} 0 & (v < v_c) \\ \pm \frac{1}{\tau} \sqrt{\frac{v}{v_c} - 1} & (v \geqslant v_c), \end{cases} \tag{3}$$

where v_c is the critical speed defined as $v_c = \frac{4a}{3\mu\tau(1-\eta_\infty/\eta_0)}$. The solution of $\omega = 0$ corresponds to the diffusive rotation. Conversely, the two nonzero solutions for $v > v_c$ indicate stationary rotation. The variation of ω with v obtained by our experiments is well fitted with Eq. (3) as shown in Fig. 3(c), where the optimal values of v_c and τ are 0.37 μm/s and 58 s, respectively. This agreement suggests that the delayed elastic force is the origin of stationary rotation as in Ref. [15]. Based on the aforementioned results, Janus particles below v_c, such as the particle shown in Fig. 2(c) with $v = 0.1$ μm/s (blue line), are expected to exhibit diffusive rotation even at large Δt.

We discuss the optimal values of v_c and τ. $v_c = 0.37$ μm/s can be obtained from its viscoelastic properties ($\eta_0 = 0.46$ Pa s, $\eta_\infty = 0.077$ Pa s, $\tau = 63$ s) and the adjustable parameter $\mu = 0.16$. Although μ should be unity because the Janus particle is subjected to the elastic force at the particle surface, the calculated value of μ is not unity. This reason is unclear at this stage. The optimal values of τ roughly agree with the values of τ obtained from the MSD of the passive particle in Appendix B. These agreement support the link between the particle dynamics and viscoelastic properties.

The effect of mode transition on the relationship between v and self-propulsion force was investigated. Since the self-propulsion force is proportional to E^2 [20], the dependence of v on E^2 was measured in water and 1.0 wt% PEO solution, as shown in Figs. 4(a) and 4(b), respectively. In water, v is proportional to E^2 as shown in Fig. 4(a), which is consistent with previous theoretical and experimental studies [20,21]. In the PEO solution, although the dependence of $v \propto E^2$ is observed at small E^2 as shown by the solid line of Fig. 4(b),

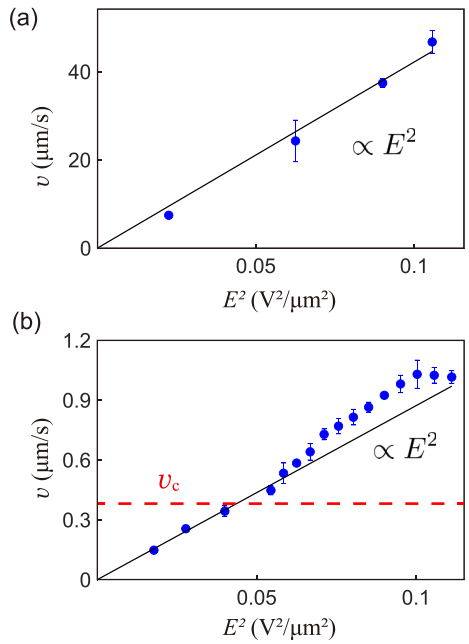

FIG. 4. Dependence of v on E^2 in water (a) and 1.0 wt% PEO solution (b). The solid lines show the best-fitted linear dependence of E^2. The dashed line in (b) represents the critical speed where the stationary rotation begins at $v_c = 0.37$ μm/s.

the dependence deviates from the line in large E^2. In large E^2, the deviation observed for v above the line indicates a decrease in viscosity, suggesting shear thinning as presented in Appendix C. Shear thinning is a characteristic of polymer solutions in which the viscosity decreases [5]. Additionally, the critical value of v, at which the deviation from the solid line begins, is approximately equal to v_c, as indicated by the dashed line in Fig. 4(b). The correspondence between the mode transition and shear thinning is discussed later.

C. Effect of viscoelasticity on mode transition

Since a delayed elastic force from the surrounding solution is required for stationary rotation, the mode transition should be determined by the viscoelasticity of the polymer solution, which is characterized by the Weissenberg number W_i. Therefore, we investigated the relationship between W_i and mode transition.

In the stationary rotation of the particle, the torque arises from the mismatch between the propulsion direction and direction of the net force from the surrounding solution owing to its viscosity and elasticity. Since the viscous resistance is instantaneous and antiparallel to the propulsion direction, misalignment does not occur when the Janus particle receives only the viscous resistance. On the other hand, since the elastic force of polymers is not instantaneous but decreases gradually over τ, the misalignment occurs when the direction of propulsion changes within τ due to thermal fluctuations and the aforementioned fluctuating flow around the particle.

For the misalignment between the propulsion directions and elastic force, the relationship between τ and traveling time over its diameter $2a/v$ is important. A slow relaxation of the elastic force with respect to $2a/v$ (i.e., $\tau > 2a/v$) leads to the the misalignment because the change in the propulsion direction is likely to occur while the elastic force remains, resulting in translational force and torque as shown in Fig. 5(a). Thus, the transition between diffusive and stationary rotation is expected to occur when $\frac{\tau}{2a/v} \sim 1$. In the context of active microrheology for viscoelastic fluids, the shear rate $\dot{\gamma}$ is considered to be $v/2a$ [25]. Thus, $\frac{\tau}{2a/v}$ can be considered as the Weissenberg number, defined as $W_i = \dot{\gamma}\tau$. Specifically, W_i was experimentally controlled between 10^{-2} and 10^{1} not only by v but also by changing C_m because τ depends on C_m [28]. The critical Weissenberg number $W_{ic} = \frac{\tau}{2a/v_c}$ for stationary rotation is calculated with the optimal values of v_c and τ obtained from our fitting results of the variation of ω with v as shown in Figs. 5(b)–5(d). Furthermore, for $C_m = 1.0$, 0.75, 0.50 and 0.25 wt%, the values of W_{ic} are 4.3 ± 0.3, 3.8 ± 0.5, 7.4 ± 2.5 and 4.3 ± 2.0, respectively. The mode transition occurs at similar W_{ic} ($W_{ic} \gtrsim 1$), strongly suggesting that the transition can be described by W_i. Additionally, it is known that non-Newtonian behavior such as shear thinning mentioned above is expected for $W_i \gtrsim 1$ [29]. The obtained W_{ic} is approximately equal to critical W_i for shear thinning. This is consistent with the results shown in Fig. 4(b), which show that shear thinning occurs in the stationary rotation region (above v_c). Furthermore, W_i for the active Brownian motion of the self-diffusiophoretic Janus particle via chemical reaction ranges from 10^{-2} to 10^{-1} [16], and W_i for the circular motion of the self-diffusiophoretic Janus particle via light irradiation exceeds 1.8 [15]. Our results with W_i ranging from 10^{-2} to 10^{1} are consistent with these two studies.

IV. CONCLUSION

The rotational motion of Janus particles in semidilute PEO solutions was examined to elucidate the effects of viscoelastic fluids on the motion of Janus particles. We used a driving method that differs from those used in the previous studies [14,16]. We investigated the self-propelled motion over a wide range of Weisenberg number W_i ranging from 10^{-2} to 10^{1} by controlling the polymer concentration C_m and particle speed v.

At small v, the rotation of the Janus particle is diffusive, and D_r was approximately a few tens of times larger than the theoretical values of thermal diffusion estimated using the Stokes-Einstein relation. At large v, the Janus particle exhibited the stationary rotation, and ω increased with increasing v. The origin of the torque for stationary rotation originates from the time-delayed restoring force arising from the polymer solution, and we quantitatively discuss the dependence of ω on v in the same way as in the previous study [15]. We find that two characteristic times are critical for the mode transition. The traveling time $2a/v$ and relaxation time of the polymer network τ and ratio $\frac{\tau}{2a/v}$ is considered as W_i. The mode transition occurred when $W_i \sim \mathcal{O}(1)$. Our explanation based on W_i is consistent with the modes reported by previous studies [15,16].

Switching of the self-propulsion modes has been reported for several types of microswimmers. A deformable microswimmer exhibits a change in trajectories from straight to circular motion, as described by Ohta-Ohkuma model [30].

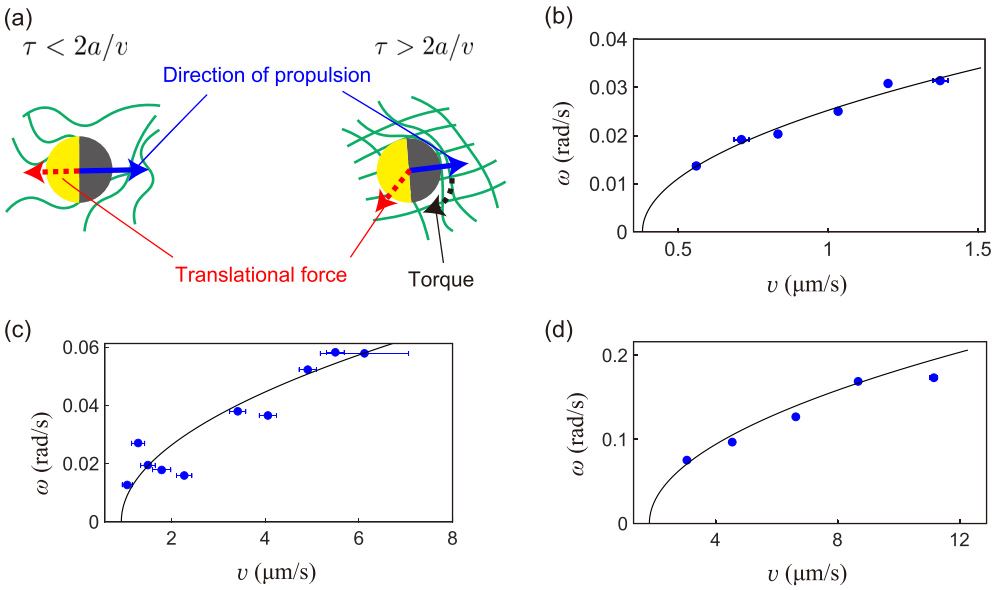

FIG. 5. Janus particles in polymeric solution at several different concentrations (C_m). (a) Schematic of two arrangements of a Janus particle in the polymeric solution. The traveling time is $2a/v$, and the relaxation time of the polymer network is τ. The green lines represent the polymers. The translational force and torque resulting from the stress acting on the Janus particle for (left) $\tau < 2a/v$ and (right) $\tau > 2a/v$. The blue arrow represents the direction of propulsion. The red and black arrows represent the translational force and torque, respectively. (b)–(d) Variation in angular frequency ω with v at C_m: (b) 0.75 wt%, (c) 0.50 wt% and (d) 0.25 wt%. The solid line represents the best-fitted curve representing Eq. (3). The optimal values of v_c and τ are (b) $v_c = 0.38$ μm/s and $\tau = 50$ s, (c) $v_c = 0.93$ μm/s and $\tau = 40$ s, (d) $v_c = 1.8$ μm/s and $\tau = 12$ s.

In this model, the mismatch between the propulsion direction and the major axis of the deformed particle is the key to circular motion. A similar transition between straight and circular motion has been reported experimentally for an oil droplet swimming in a surfactant solution [31]. A nematic liquid crystal (NLC) droplet swimming in a surfactant solution exhibits motion switching between straight, helical, and random with velocity [32]. In this case, the misalignment of the point defect within a droplet induces asymmetric convective flow within the droplet. In all the aforementioned cases, the origin of the transition is attributed to the internal degree of freedom of the particle, such as the deformation of the droplet or the change in the orientation of the LC molecules. In the present system, on the other hand, the transition is caused by the change in the mechanical response of the surrounding fluid. Considering that the response (a self-propelled particle or surrounding fluids) is important for mode transition, our system is complementary to studies on deformable droplets and NLC droplet systems. Our results suggest that the responsiveness of the self-propelled object and surrounding fluid leads to a mode transition.

Our study showed that viscoelasticity plays an important role in determining the kinetic mode of self-propelled particles. Our results will be useful in various research areas, including biological phenomena and microfluidic engineering of viscoelastic fluids. Additionally, our system can be used as a chiral active matter with a controlled activity.

ACKNOWLEDGMENTS

This work was supported by JSPS KAKENHI Grants (No. 17H02944 and No. 20H01873) and JSPS Core-to-Core Program "Advanced core-to-core network for the physics of self-organizing active matter (JPJSCCA20230002)". K.S. appreciates K. Ohnishi and R. Iimori for the sample cell trials. K.S. thanks JST SPRING (Grant No. JPMJSP2136) and a Grant-in-Aid for JSPS Fellows (Grants No. 22J10770 and No. 24KJ0235).

APPENDIX A: DISTRIBUTIONS OF SELF-PROPULSION SPEED

We summarize average speed, standard deviations, and numbers of samples at each C_m in Table I.

APPENDIX B: ESTIMATION OF THE ZERO-SHEAR VISCOSITY η_0 IN THE PEO SOLUTION

Before estimating η_0 in the PEO solution, we compare the translational diffusion coefficient D_t^0 of a probe particle in water estimated by the mean-squared displacement (MSD) $\langle \Delta \boldsymbol{r}(t)^2 \rangle$ of the particle, $\langle \Delta \boldsymbol{r}(t)^2 \rangle = 4D_t^0 \Delta t$, with the theoretical value by the Stokes-Einstein relation

TABLE I. Average speed v_{av}, standard deviation Δ, and number of samples N of the distributions of self-propulsion speed at $E = 0.17$ V/μm.

C_m (wt%)	v_{av} (μm/s)	Δ (μm/s)	N
1.0	0.44	0.23	38
0.75	0.80	0.31	34
0.50	2.8	1.1	35
0.25	10	3.5	60

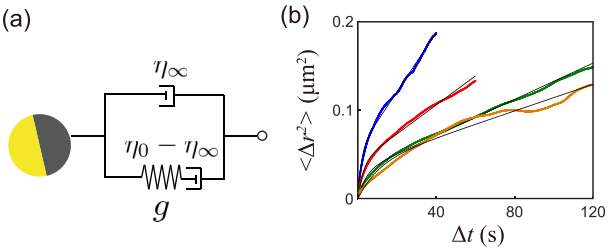

FIG. 6. Microrheological measurement of a PEO solution. (a) Schematic for mechanical representation of the solution, comprising a dashpot (the instantaneous viscosity η_∞) and a Maxwell combination in series of an elastic element (stiffness g) and a dashpot (viscosity $\eta_0 - \eta_\infty$) with relaxation time $\tau = (\eta_0 - \eta_\infty)/g$ with the zero-shear viscosity η_0. (b) Mean-squared displacement $\langle \Delta \boldsymbol{r}^2 \rangle$ of a silica particle with 5 μm diameter at (yellow) $C_\mathrm{m} = 1.0$ wt%, (green) 0.75 wt%, (red) 0.50 wt% and (blue) 0.25 wt%. The solid lines are the best-fitted curves of Eq. (A1). The optimal values are $\eta_\infty = 0.077$ Pa s, $\eta_0 = 0.46$ Pa s and $\tau = 62$ s (yellow); $\eta_\infty = 0.041$ Pa s, $\eta_0 = 0.34$ Pa s and $\tau = 34$ s (green); $\eta_\infty = 0.021$ Pa s, $\eta_0 = 0.21$ Pa s and $\tau = 28$ s (red); $\eta_\infty = 0.0099$ Pa s, $\eta_0 = 0.10$ Pa s and $\tau = 18$ s (blue).

$D_t^0 = \frac{k_\mathrm{B}T}{6\pi\eta_0 a}$ as a sanity check. The value of D_t^0 estimated by MSD is 8.0×10^{-2} μm^2/s. This value is slightly smaller than the theoretical value $\frac{k_\mathrm{B}T}{6\pi\eta_0 a} = 9.8 \times 10^{-2}$ μm^2/s with $T = 25$ °C, $\eta_0 = 0.89$ mPa s and $a = 2.5$ μm. Since the particle settles down near the cell bottom, the particle-wall interaction decreases the effective translational diffusion coefficient [33]. Thus, we consider that our system does not have problems.

We estimate η_0 by fitting the MSD of the probe particle obtained to the theoretical MSD calculated using the Jeffreys model for polymer solutions, as Fig. 6(a) [14]:

$$\langle \Delta \boldsymbol{r}(t)^2 \rangle = 4D_t^0 \left[t + \left(1 - \frac{\eta_\infty}{\eta_0} \right) \tau (1 - e^{-t/\lambda}) \right], \quad \text{(B1)}$$

where $D_t^0 = k_B T/6\pi a \eta_0$, $\lambda = (\eta_\infty/\eta_0)\tau$ and $\tau = (\eta_0 - \eta_\infty)/g$. Brownian motion of a silica particle of 5 μm diameter dispersed in PEO solutions is observed, and its MSD is fitted by Eq. (A1), as shown in Fig. 6(b).

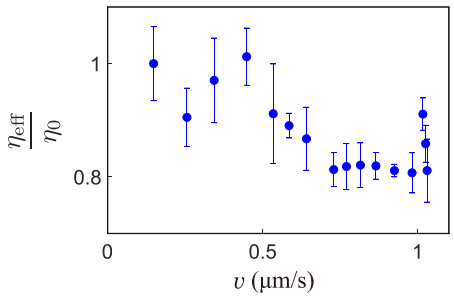

FIG. 7. Variation of $\frac{\eta_\mathrm{eff}}{\eta_0}$ with v at $C_\mathrm{m} = 1.0$ wt%.

APPENDIX C: RATIO OF EFFECTIVE VISCOSITY η_eff TO η_0 IN A PEO SOLUTION

The ratio of effective viscosity η_eff to η_0 is estimated from the balance between the self-propulsion force by ICEP and the viscous drag force ($6\pi\eta_\mathrm{eff} a v$). The self-propulsion speed v is proportional to E^2 [21], $v = \alpha E^2$, with a constant α. α is estimated by the linear fit to the data in Fig. 4(b) below v_c, and thus the self-propulsion force can be estimated as $6\pi\eta_0 a \alpha E^2$ by Stokes low with viscosity η_0 in $v < v_\mathrm{c}$. The balance between the self-propulsion force and the viscous drag force gives $\frac{\eta_\mathrm{eff}}{\eta_0} = \frac{\alpha E^2}{v}$. $\frac{\eta_\mathrm{eff}}{\eta_0}$ decreases in larger v as shown in Fig. 7, suggesting shear thinning in large v.

[1] J. Elgeti, R. G. Winkler, and G. Gompper, Rep. Prog. Phys. **78**, 056601 (2015).
[2] C. Bechinger, R. Di Leonardo, H. Löwen, C. Reichhardt, G. Volpe, and G. Volpe, Rev. Mod. Phys. **88**, 045006 (2016).
[3] G. Li, E. Lauga, and A. M. Ardekani, Fluid Mech. **297**, 104655 (2021).
[4] L. S. Hirst, *Fundamentals of Soft Matter Science* (CRC Press, Boca Raton, FL, 2019).
[5] R. G. Larson, *The Structure and Rheology of Complex Fluids* (Oxford University Press, New York, 1999).
[6] A. Patteson, A. Gopinath, M. Goulian, and P. Arratia, Sci. Rep. **5**, 15761 (2015).
[7] S. Liu, S. Shankar, M. C. Marchetti, and Y. Wu, Nature (London) **590**, 80 (2021).
[8] A. C. H. Tsang, E. Demir, Y. Ding, and O. S. Pak, Adv. Intell. Syst. **2**, 1900137 (2020).
[9] J. Katuri, X. Ma, M. M. Stanton, and S. Sánchez, Acc. Chem. Res. **50**, 2 (2017).
[10] P. G. de Gennes, Angew. Chem. Int. Ed. Engl. **31**, 842 (1992).
[11] A. Walther and A. H. E. Muller, Chem. Rev. **113**, 5194 (2013).
[12] W. Wang, X. Lv, J. L. Moran, S. Duan, and C. Zhou, Soft Matter **16**, 3846 (2020).
[13] J. R. Howse, R. A. L. Jones, A. J. Ryan, T. Gough, R. Vafabakhsh, and R. Golestanian, Phys. Rev. Lett. **99**, 048102 (2007).
[14] J. R. Gomez-Solano, A. Blokhuis, and C. Bechinger, Phys. Rev. Lett. **116**, 138301 (2016).
[15] N. Narinder, C. Bechinger, and J. R. Gomez-Solano, Phys. Rev. Lett. **121**, 078003 (2018).
[16] S. Saad and G. Natale, Soft Matter **15**, 9909 (2019).
[17] H-R. Jiang, N. Yoshinaga, and M. Sano, Phys. Rev. Lett. **105**, 268302 (2010).
[18] I. Buttinoni, G. Volpe, F. Kümmel, G. Volpe, and C. Bechinger, J. Phys.: Condens. Matter **24**, 284129 (2012).
[19] J. Palacci, C. Cottin-Bizonne, C. Ybert, and L. Bocquet, Phys. Rev. Lett. **105**, 088304 (2010).
[20] T. M. Squires and M. Z. Bazant, J. Fluid Mech. **560**, 65 (2006).
[21] S. Gangwal, O. J. Cayre, M. Z. Bazant, and O. D. Velev, Phys. Rev. Lett. **100**, 058302 (2008).
[22] A. Boymelgreen, G. Yossifon, and T. Miloh, Langmuir **32**, 9540 (2016).
[23] C. H. Lin, Y. L. Chen, and H. R. Jiang, RSC Adv. **7**, 46118 (2017).

[24] E. Andablo-Reyes, P. Díaz-Leyva, and J. L. Arauz-Lara, Phys. Rev. Lett. **94**, 106001 (2005).
[25] J. R. Gomez-Solano and C. Bechinger, Europhys. Lett. **108**, 54008 (2014).
[26] C. Lozano, J. R. Gomez-Solano, and C. Bechinger, Nat. Mater. **18**, 1118 (2019).
[27] Y. L. Raikher, V. V. Rusakov, and R. Perzynski, Soft Matter **9**, 10857 (2013).
[28] J. H. van Zanten, S. Amin, and A. A. Abdala, Macromolecules **37**, 3874 (2004).
[29] J. R. Gomez-Solano and C. Bechinger, New J. Phys. **17**, 103032 (2015).
[30] T. Ohta and T. Ohkuma, Phys. Rev. Lett. **102**, 154101 (2009).
[31] F. Takabatake, N. Magome, M. Ichikawa, and K. Yoshikawa, J. Chem. Phys. **134**, 114704 (2011).
[32] M. Suga, S. Suda, M. Ichikawa, and Y. Kimura, Phys. Rev. E **97**, 062703 (2018).
[33] J. Happel and H. Brenner, *Low Reynolds Number Hydrodynamics: With Special Applications to Particulate Media* (Springer, New York, 1981).